FLEXIBLE PARYLENE ACTUATOR FOR MICRO ADAPTIVE FLOW CONTROL

T. N. Pornsin-Sirirak, Y.C. Tai
Caltech Micromachining Laboratory,
Electrical Engineering Department, California Institute of Technology
Pasadena, CA 91125

H. Nassef, C.M. Ho
Mechanical and Aerospace Engineering,
University of California,
Los Angeles, CA 90095

ABSTRACT

This paper describes the first flexible parylene electrostatic actuator valves intended for micro adaptive flow control for the future use on the wings of micro-air-vehicle (MAV). The actuator diaphragm is made of two layers of parylene membranes with offset vent holes. Without electrostatic actuation, air can move freely from one side of the skin to the other side through the vent holes. With actuation, these vent holes are sealed and the airflow is controlled. The membrane behaves as a complete diaphragm.

We have successfully demonstrated this function using a 2-mm x 2-mm parylene diaphragm electrostatic actuator valves. This work also includes the novel anti-stiction technology that is crucial to make such large-area parylene actuator diaphragm with the combined use of anti-stiction posts, self-assembled monolayers (SAM), surface roughening, and bromine trifluoride (BrF_3) dry etching. With the help of SAM treatment, the operating voltage is lowered from 30 volts to 13 volts. The load deflection method is then used to measure the effective thickness of the composite diaphragm. The flexible parylene diaphragm can be deflected up to 100 μm when 150 Torr of pressure is applied. The result is fitted into a theoretical model and yields an effective thickness of 5.9 μm, which is agreeable with the actual thickness of 5.6 μm, thus proves the functionality of the device.

INTRODUCTION

Previous year in MEMS 2000, we reported a MEMS wing technology using titanium-alloy and parylene as wing spars and membrane, respectively [1]. Our further wind tunnel experiments have indicated that aerodynamic thrust force produced by flapping are intimately related to the flexibility and the location of the wing membrane [2]. The comparison of the thrust performance of flexible wing membrane to the rigid wing membrane is shown in Figure 1. The mylar wing, which is less rigid and has better flexibility than the paper wing, shows to have higher thrust coefficient, hence higher thrust force, when it is compared to the more rigid paper wing.

We have also discovered the effect of the inboard and outboard regions of the wing in relation to thrust and lift generations. This effect is shown in Figure 2. Two wings are compared where the inboard region of one wing was arbitrarily

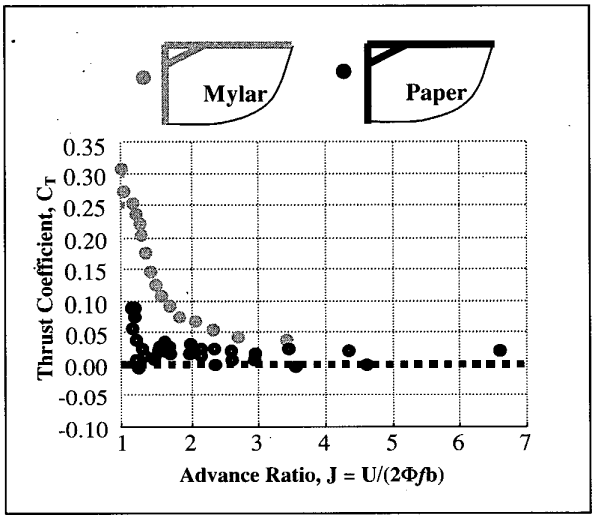

Figure 1. *Aerodynamics thrust performance of wings with different membrane rigidity*

removed. Because the wing speed varies along the wing span, the strength of the dynamic stall vortex also varies, and thus the lift force. The rotational speed of the wings is higher towards the tips and this leads to stronger amounts of vorticity in the outboard region of the wings. Therefore, it can be expected that the bulk of the lift is produced in the outboard region of the wings. Removal of the inboard region does not affect the lift coefficient as shown in Figure 2a) because the outboard vorticity is not affected. However, the thrust production is affected dramatically as seen in Figure 2b). The thrust performance of the wing without the inboard region deteriorates when compared to that of the wing with the inboard region, which is yet another indication of the dependence of thrust on the vortex shedding. This indicates the area where the actuators can be distributed to control the flexibility of the membrane and how the vortices are shed. Hence, the thrust performance can be improved.

This is the motivation to investigate the flexible parylene MEMS actuator membrane for micro adaptive flow control. By distributing actuators on the wing membrane, it is possible to have

0-7803-5998-4/01/$10.00 @2001 IEEE

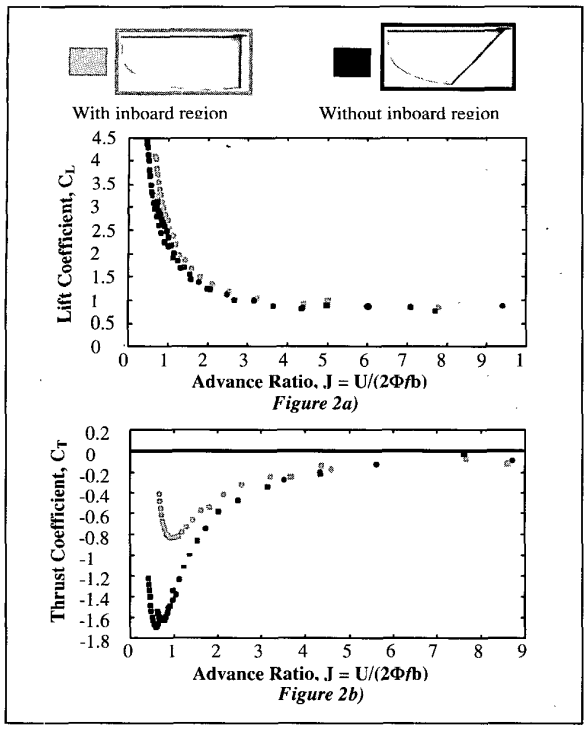

Figure 2. *Aerodynamics thrust performance of wings with different membrane rigidity*

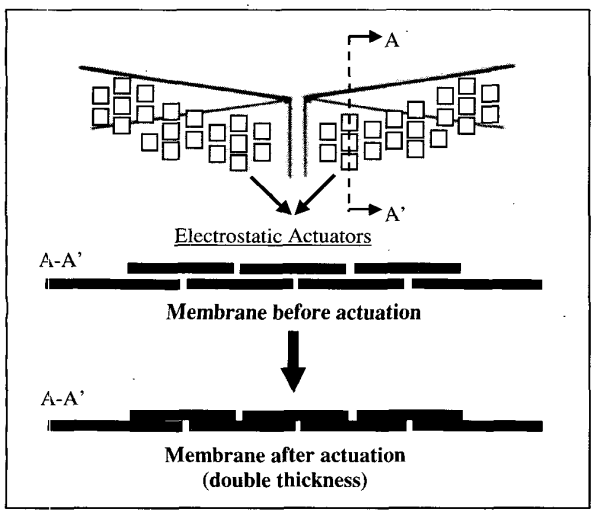

Figure 3: *Active wing actuator membrane concept*

an active control of the flexibility of the wings to achieve optimal aerodynamic performance. This concept is illustrated in Figure 3. Before actuation, the offset vent holes on the diaphragm let the air move freely through the membrane; the membrane remains flexible. Once actuated, the holes are sealed and the membrane behaves as a complete diaphragm. The thickness is also doubled. Therefore, the rigidity of the membrane increases; this will affect the thrust performance. This kind of membrane will have important application for adaptive airfoil that its wing loading can be controlled by simple electrostatic actuation. To demonstrate this feasibility, flexible parylene actuator membrane is built on a silicon chip. It will be demonstrated that the effective thickness of the parylene composite membrane changes after an actuation is performed. The load deflection test setup is built to collect data that will be fitted into the load deflection model [3].

DESIGN AND FABRICATION

The large-area of 2-mm x 2-mm parylene electrostatic actuator diaphragm is fabricated and shown in Figure 4. The diaphragm is consisted of two metalized parylene membranes, each with 2.8-μm thickness. Photoresist (4 μm) is used as a sacrificial layer by acetone dissolution. Because parylene has a low Young's modulus (~4.5 GPa), acetone surface tension can easily pull down the structure to substrate to cause stiction. These challenges must be overcome. The anti-stiction technology we developed is a combination of steps that use both wet photoresist dissolution and silicon dry etching in BF_3. Photoresist dissolution allows large-area parylene membrane release and BF_3 dry etch prevents stiction. We also utilize anti-stiction posts to reduce the collapse of the top parylene membrane after wet releasing of photoresist. Surface of parylene is roughened in O_2 plasma to reduce the contact area of stiction. In addition, after releasing photoresist, SAM coating of octadecyltrichlorosilane (OTS) [4, 5] is used to treat the parylene surface to further reduce possible stiction.

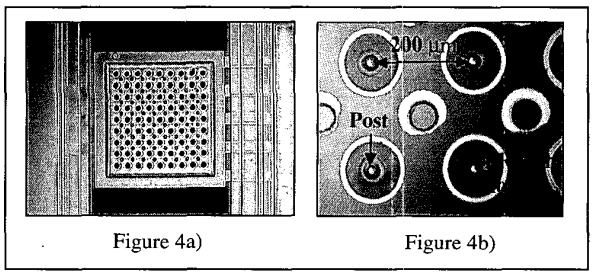

Figure 4: *a) fabricated 2-mm x 2-mm parylene electrostatic actuator diaphragm; b) anti-stiction posts and photoresist dissolution holes*

The actuator diaphragm fabrication process is shown in Figure 5. First, 1.8-μm thermal oxide is grown at 1050°C by wet oxidation. This layer is used as a mask during formation of the diaphragm by KOH etching. The oxide is patterned from the backside. Then the substrate is time-etched in KOH solution at 58°C for 23 hours to form a thin 25-um-thick silicon diaphragm. This is followed by the front-side patterning of the remaining oxide to create membrane area of 2-mm x 2-mm. The surface is then roughened with a 3 mTorr pulse of BrF_3. This helps improve the adhesion of parylene to the substrate surface. Next, the solution of 0.5% A-174 silane adhesion promotion (DI H_20: IPA: A-174 = 100:100:1 in volume) is used to further improve the adhesion. A-174 is commercially available and can be obtained

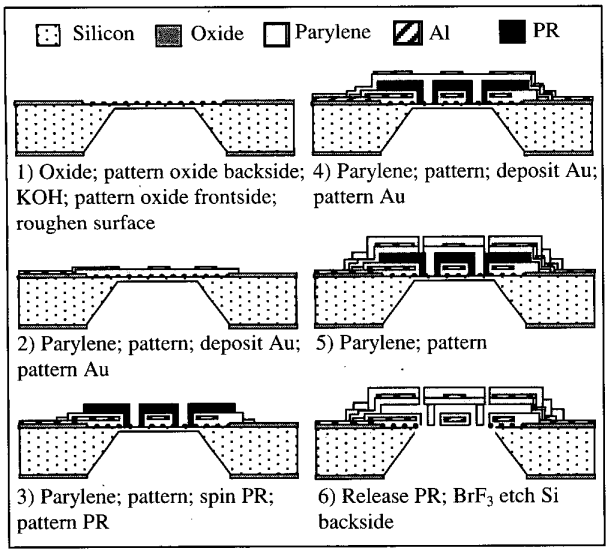

Figure 5: *Fabrication process for flexible parylene electrostatic actuator diaphragm*

from Specialty Coating Systems, Inc. [6] The solution is stirred for at least 30 seconds and allowed to settle for a minimum of 2 hours. The wafers are then submerged in the prepared solution for 15 minutes and air dried for another 15 minutes. Then they are rinsed with IPA for 15-30 seconds and dried in a convection oven for 30 minutes at 70°C.

Next, the first thin film layer of parylene C is deposited and patterned, followed by parylene surface roughening by O_2 plasma. Cr/Au/Cr layers, as ground electrodes, are evaporated and patterned. We use Cr/Au/Cr layers because A-174 silane adhesion promotion will create a good bonding strength between CrO_2 and parylene interface to improve adhesion. The use of O_2 plasma to roughen the parylene surface before depositing Cr layer is also important because without roughening the surface, we have experienced the delamination of metal layers due to poor adhesion. The next layer of parylene is then deposited to seal the ground electrode. This helps prevent short-circuiting the ground and top electrodes.

After spinning on the 4-μm-thick sacrificial layer photoresist, the resist is patterned to form anti-stiction posts. The post size is 20-μm in diameter and 200-μm apart. The third layer of parylene is then deposited and the surface is roughened. Top Cr/Au/Cr layers are evaporated and patterned, followed by the deposition of the last parylene layer. Finally, the top parylene membrane is patterned to open up areas for electrode contacts and holes for photoresist dissolution in acetone. The wafers are then submerged in acetone to release the diaphragm. After releasing the diaphragm, we also submerge the wafers in SAM solution of octadecyltrichlorosilane (OTS) to further prevent stiction.

It is important to note that if there are no posts between the top and the bottom parylene membranes, we have yet been able to successfully free a large area of parylene without stiction. As shown in Figure 6, without anti-stiction posts, the top layer of parylene on a test structure is pulled down by meniscus force after the dissolution of photoresist in acetone. The anti-stiction posts, which are rested on a thin 20-μm-thick silicon diaphragm, prevent the stiction. This thin silicon diaphragm is then released by BrF_3 dry etching [7]. The dry etching is necessary at the last step because the membranes will not be in contact with any wet chemicals that can cause stiction to occur.

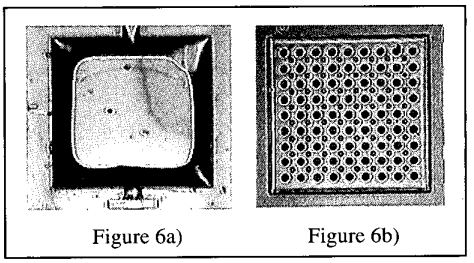

Figure 6: a) stiction occurred on a 400-μm x 400-μm parylene diaphragm when no posts and any anti-stiction methods used; b) no stiction occurred for a 2-mm x 2-mm parylene diaphragm when posts and other stiction preventive methods are used.

RESULTS AND DISCUSSION

The actuation test results show that without SAM coating, a higher voltage must be applied in order to actuate the parylene diaphragm actuators. This actuation voltage is 30 volts. With SAM coating, the actuation voltage is reduced to 13 volts. The load deflection test setup is constructed. By applying pressure to the backside of the membrane, the deflection distance can be measured by the load deflection setup before and after actuation. Before actuation, the vent holes open; the membrane is flexible. After actuation, the vent holes are closed. Thus the airflow is ceased and can be controlled. The membranes become more rigid. The result is shown in Figure 7. The actuation effect on the stiffness of the membrane can be seen clearly.

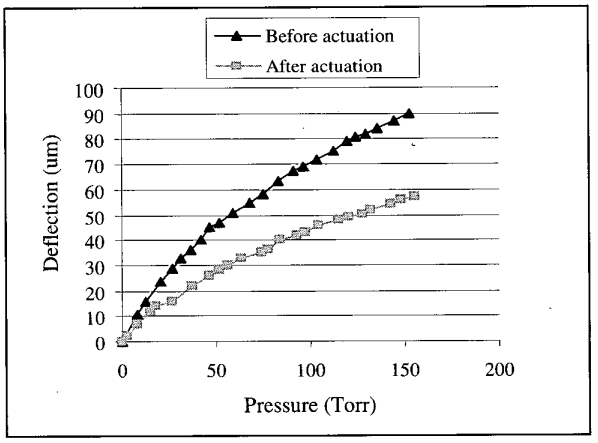

Figure 7: *Load deflection test result indicates the stiffness change after actuation*

Figure 8 shows the after-actuation data fitted by the load deflection for rectangular membrane model. We assume that our

membrane behaves as a rectangular membrane once the actuation occurs. The relationship between the pressure, p, and the deflection height, h, is shown in the following equation:

$$P = \frac{C_1 \sigma t h}{a^2} + \frac{C_2 E t h^3}{a^4} \quad (1)$$

where

$$C_1 = \frac{\pi^4 (1+n^2)}{64},$$

$$C_2 = \frac{\pi^6}{32(1-v^4)}\{\frac{9+2n^2+9n^4}{256} - [\frac{(4+n+n^2+4n^3-3nv(1+n))^2}{2\{81\pi^2(1+n^2)+128n+v[(128n-9\pi^2(1+n^2)]\}}]\},$$

$n = 1$;

$v = 0.25$

σ = int *ernal stress*; t = *the membrane thickness*

a = *half − length of the membrane*

E = *Young's* mod *ulus*

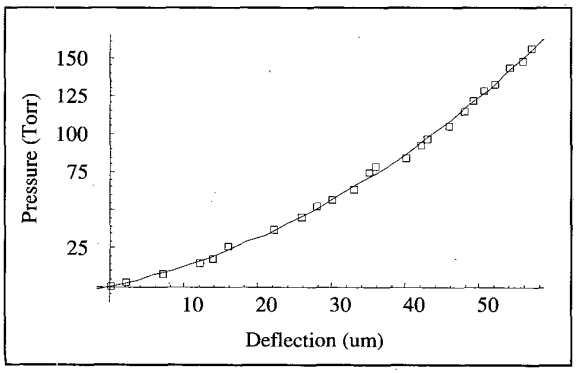

Figure 8: *Plot of pressure, p, vs. deflection height,h, of the after-actuation for flexible parylene actuator membranes*

From Figure 8, the model fit yields,

$$P = \underbrace{1.561}_{A} * h + \underbrace{0.000363}_{B} * h^3 \quad (2)$$

The effective thickness after actuation can be calculated by ,

$$\textit{Effective thickness } t = \frac{Ba^4}{C_2 E} \quad (3)$$

where B = 0.000363, a = 1 mm, C_2 = 1.83, and E = 4.5 GPa (Young's modulus of parylene). This yields the calculated effective thickness of 5.9 μm compared to the actual diaphragm thickness of 5.6 μm. which is agreeable and the functionality of this flexible parylene actuator diaphragm is proved.

CONCLUSIONS

We have successfully fabricated 2-mm x 2-mm parylene diaphragm electrostatic actuator valves and used this flexible parylene actuator for micro adaptive flow control. This work also includes the novel anti-stiction technology that is crucial to make such large-area parylene actuator diaphragm with the combined use of anti-stiction posts, SAM layers, surface roughening, and bromine trifluoride (BrF_3) dry etching. The operating voltage of this device can be initiated at 13 volts. The effective thickness of the composite diaphragm is calculated by fitting the load-deflection test data into a theoretical model and it yields an effective thickness as 5.9 μm, which is very close with the actual measured thickness of 5.6 μm.

To further improve the aerodynamic performance of MEMS wings, the selective stiffness distribution control on the membrane is desired. This will help control the flexibility of the wings and how vortices are shed. Thus our future work is to integrate these flexible actuator membranes onto the membrane of MEMS wings.

ACKNOWLEDGEMENTS

This work is supported under DARPA/TTO MAV program DABT63-98-C-0005. The authors would like to thank Dr. Xing Yang from Caltech for his assistance in load deflection test and Steve Ho from UCLA for his assistance in the wind tunnel testing and his contributions to the project.

REFERENCES

1. T. N. Pornsin-Sirirak, S.W. Lee, H. Nassef, J. Grasmeyer, Y.C. Tai, C. M. Ho, M. Keennon, "MEMS Wing Technology for a Battery-Powered Ornithopter," *Proceedings of the 13th IEEE Annual International Conference on MEMS 2000*, Miyazaki, Japan, 1/23-27/00, pp. 799 - 804

2. T. N. Pornsin-Sirirak, Y.C. Tai, H. Nassef, C. M. Ho, "Unsteady-State Aerodynamic Performance of MEMS Wings," *International Symposium on Smart Structures and Microsystems 2000 (IS3M)*, The Jockey Club, Hong Kong, 10/19-21/00, pp. G1-2

3. O. Tabata, K. Kanahata, S. Sugiyama, I. Igarashi, "Mechanical Property Measurements of Thin Films Using Load-Deflection of Composite Rectangular Membranes," *Sensors and Actuators, 20 (1989)*, pp. 135 – 141

4. R. Maboudian, "Self-Assembled Monolayers as Anti-Stiction Coatings for Surface Microstructures," *Digest of Technical Papers, The 10th International Conference on Solid-State Sensors and Actuators (Transducer'99)*, Sendai, Japan, 6/7-10/99, Vol 1, pp. 22-25

5. M.R. Houston, R. Maboudian, R. T. Howe, "Self-Assembled Monolayer Film as Durable Anti-Stiction Coatings for Polysilicon Microstructures", *Solid-State Sensor and Actuator Workshop*, Hilton Head, South Carolina, 6/2-6/96, pp. 42 – 47

6. Product Specifications, " A-174 Silane Promotion", *Specialty Coating Systems, Inc.* Indianapolis, IN, 1-800-356-8260

7. X. Q. Wang, X. Yang, K. Walsh, and Y. C. Tai, "Gas-Phase Silicon Etching with Bromine Trofluoride," *Digest of Technical Papers, The 9th International Conference on Solid-State Sensors and Actuators (Transducers '97)*, Chicago, IL, 6/ 16-19/97, Vol. 2, pp. 1505-1508